Phys. Lett. B 874 (2026) 140214

Contents lists available at ScienceDirect

Physics Letters B

journal homepage: www.elsevier.com/locate/physletb

Letter

Resonant states in three- and four-body hypernuclear systems

Rimantas Lazauskas [a], Arnoldas Deltuva [b,*], Daniel Gazda [c], Martin Schäfer [c]

[a] PHC, CNRS/IN2P3, Université de Strasbourg, 23 Rue du Loess, 67037, Strasbourg, France
[b] Institute of Theoretical Physics and Astronomy, Vilnius University, Saulėtekio alėja 3, LT-10257, Vilnius, Lithuania
[c] Nuclear Physics Institute, Czech Academy of Sciences, 25068, Řež, Czech Republic

ARTICLE INFO

Editor: Baha Balantekin

Keywords:
Hypernuclear interactions
Faddeev-Yakubovsky equations
Resonant states

ABSTRACT

Using realistic nuclear and hyperon–nucleon interactions obtained from chiral effective field theory, we explore the possible existence of resonant states in three- and four-body strangeness S = -1 hypernuclear systems. In particular, we focus on Feshbach resonant states near the Σ-hyperon production threshold. We firmly identified $J^\pi = 1/2^+$ ΣNN as well as $J^\pi = 0^+$ ΣNNN states and determined their positions and widths to draw conclusions on their experimental observability.

1. Introduction

Hypernuclei offer valuable insights into the fundamental baryonic interactions which govern both nuclear matter and phenomena occurring in astrophysical environments, such as neutron stars. In the past, hypernuclei were investigated through cosmic ray reactions and accelerator-based experiments [1]. More recently, production of strange particles in relativistic heavy-ion and particle colliders have ushered in a new era of hypernuclear research [2–4], unveiling intriguing and often puzzling results [5–8]. Unlike the rather well-established nucleon–nucleon (NN) interactions, the hyperon–nucleon (YN) interactions are constrained by only about 35 data points for scattering total cross sections at lower energies. Theoretical modeling of the YN interactions is even more challenging due to the presence of strongly coupled ΛN and ΣN channels, separated by a mere ≈ 80 MeV. This coupling amplifies effects that are less prominent in non-strange ordinary nuclei [9–11], such as three-body forces and charge symmetry breaking. In particular, differences in the Λ separation energies of mirror hypernuclei, such as ${}^{4}_{\Lambda}$He and ${}^{4}_{\Lambda}$H, challenge our current understanding of the nuclear strong interaction [12–15].

Strangeness S = -1 hypernuclear systems containing a Σ hyperon (often loosely termed as Σ hypernuclei) represent a relatively unexplored yet important area of research, particularly because of their potential to reveal new aspects of the elusive YN interactions, a key objective of strangeness nuclear physics. Study of Σ-hypernuclear states could enhance our understanding of YN interactions, particularly in the less-known ΣN sector, and contribute significantly to a more comprehensive view of both few- and many-body systems. Moreover, these quantum systems also reveal intriguing dynamics. The strong-interaction $\Sigma N - \Lambda N$ conversion can only lead to short-lived Feshbach resonances near the Σ-production threshold, rather than Σ-hypernuclear bound states. However, despite decades of theoretical and experimental efforts, the existence of Σ-hypernuclear states remains controversial [16–20]. While several measurements reported candidate Σ-hypernuclear states [21,22], the absence of well-defined ground states continues to pose significant challenges. There are several ongoing studies using correlation femtoscopy [23], as well as experiments based on (K^-, π) reactions [24,25] aiming to reveal the presence of the lightest Σ-hypernuclear states. In line with these efforts we aim to explore presence of Feshbach resonant states near the Σ hyperon production threshold in $A = 3, 4$ S = -1 hypernuclei. By addressing these questions, we provide new insights into the nature of hypernuclear states and their broader implications for nuclear physics and astrophysics.

2. Methods

Given the complexity of the calculations, we validated our results by employing two independent computational methods. The A = 3 systems were analyzed by solving the Faddeev-Merkuriev (FM) equations in configuration space [26] and the Alt–Grassberger–Sandhas (AGS) equations in momentum space [27]. For the four-body problem, we utilized the Faddeev–Yakubovsky (FY) equations in configuration space [28].

* Corresponding author.
E-mail address: arnoldas.deltuva@tfai.vu.lt, deltuva@campus.ul.pt (A. Deltuva).

https://doi.org/10.1016/j.physletb.2026.140214
Received 29 October 2025; Received in revised form 9 December 2025; Accepted 25 January 2026
Available online 30 January 2026

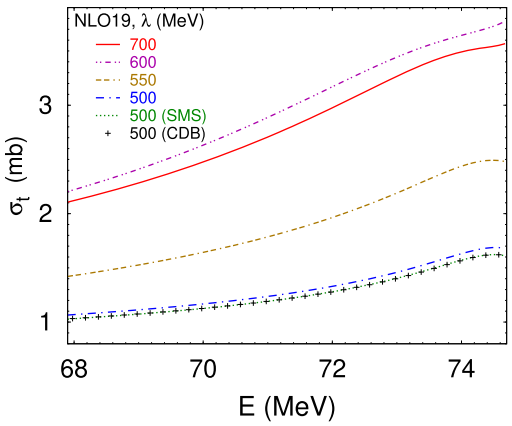

Fig. 1. Total cross section (σ_t) for Λ–deuteron scattering in the $J^\pi=1/2^+$ state below the Σ^0–^{2}H threshold at 74.73 MeV. Predictions using the Idaho-N3LO *NN* potential [39] and NLO19 *YN* [38] potentials with different λ cutoffs are compared. For λ=500 MeV also results with chiral SMS and CD-Bonn potentials are shown.

To account for the coupling between the $(\Lambda N, \Sigma^+ N, \Sigma^0 N, \Sigma^- N)$ channels and the mass differences among $\Lambda - \Sigma^+ - \Sigma^0 - \Sigma^-$, the problem was approached in an extended Hilbert space consisting of multiple sectors, akin to methods used for addressing the Δ isobar [29] or nuclear core excitations [30,31]. In order to determine the positions of resonances, we applied the Complex Scaling Method (CSM) in configuration space [32]. Alternatively, the AGS equations were solved at real energies, and the complex energy/momentum poles, which indicate the positions of resonant states, were determined by analyzing the energy-dependence of *YNN* transition operator matrix elements [33,34]. This method circumvents the need for CSM. Remarkable numerical consistency between the results of the AGS and FM/FY methods ensured the determination of pole positions up to few keV.

Notably, neutrons, protons, and strange baryons were treated as distinct particles by considering their physical masses and without relying on isospin symmetry. This approach allowed to preserve the physical threshold positions for all multi-particle channels. We refer to our previous works [30–33,35] for more details on the numerical techniques.

3. Results

We employ *YN* interactions constructed by the Jülich–Munich group [11,36–38], derived within $SU(3)$ χEFT up to leading order (LO) and next-to-leading order (NLO), and fitted to low-energy ΛN and ΣN scattering data. The NLO models also include charge symmetry breaking by introducing additional contact interaction terms adjusted to reproduce the $^4_\Lambda$He and $^4_\Lambda$H binding energy difference [11].

Our analysis of resonant *YNN* and *YNNN* systems indicates only a marginal sensitivity to the choice of *NN* interaction—whether AV18 [40], CD-Bonn [41], Idaho-N3LO [39], or Bochum N4LO+ (SMS) [42]—despite the differences in the structure and calibration of these models. Similar conclusions were reported in [43–45], where extensive sensitivity study of Λ-hypernuclear observables to nuclear interactions linked this insensitivity to the weak binding of the Λ hyperon. In contrast, Fig. 1 demonstrates that the total (elastic plus break-up) Λ–deuteron (^{2}H) cross section exhibits a pronounced dependence on the choice of *YN* interaction. The total cross sections for the NLO19 *YN* model [38] with regulator cutoff λ=600 MeV are twice as large as for λ=500 MeV. Consequently we focus on *YN*-model dependence adopting the Idaho-N3LO *NN* interaction [39] along with *NNN* interaction of [46].

3.1. $A = 3$ hypernuclear resonances

Our findings align with previous studies [47–51] on the possible existence of three-body hypernuclear states with charges Z=0 and Z=2 near the Λnn and Λpp thresholds, respectively. Binding these systems without forming a ΛN bound states requires a significant fine-tuning of the *YN* interaction. The most favorable configuration with $J^\pi=1/2^+$ is dominated by total orbital momentum $L^\pi=0^+$ components and is supported by a weak centrifugal barrier. A slight reduction in the interaction strength from the critical value, corresponding to an infinitesimally weakly bound trimer, leads to the formation of very fragile resonant states that quickly dissolve into the continuum. This critical phenomenon, characteristic of Efimov physics [52,53], is well documented and not elaborated further here.

Next, we focus on Σ-hypernuclear states. For systems lacking a pronounced resonant behavior, a systematic method to identify and study S-matrix poles is interaction scaling, as applied e.g. in three/four-neutron scenarios [33,54–56]. Additionally, interaction scaling is useful for examining various pole types, such as bound, unstable, virtual, and resonant states; especially when the interaction strength has uncertainties or is altered by external fields, like in cold-atom systems [34,57,58]. S-matrix pole positions E_R+iE_i and k_R+ik_i in the energy and momentum complex planes correspond via $(k_R+ik_i)^2/2\mu_{XY}=E_R+iE_i-E_{XY}$, where E_{XY} is the $X+Y$ subsystems threshold energy and μ_{XY} their reduced mass. To support a resonant state formation, we adjust the *YN* interaction by scaling the $V_{\Sigma' N',\Sigma N}$ components by a factor γ, leaving $V_{\Lambda N',\Sigma N}$ and $V_{\Lambda N,\Lambda N}$ unchanged. Such a strategy enables one to smoothly increase the Σ–nuclear attraction, while minimizing the effects on the better-constrained ΛN interaction and the impact on Λ-hypernuclear properties. Additionally, this modification preserves the isospin dependence of the ΣN interaction. Physical predictions are recovered for $\gamma\to1$. In Fig. 2, the trajectory of a $^3_\Sigma$H pole with total charge Z=1 and $J^\pi=1/2^+$ is shown when γ is varied in the interval (1.45, 1). For γ=1.35, all considered *YN* interaction models support a Feshbach resonant state below the Σ^0–^{2}H threshold. Despite lying below the Σ^0–^{2}H threshold, this state is unstable and decays by emitting a Λ hyperon. Nevertheless, due to the significant mass difference between Σ^0 and Λ hyperons, the overlap between the loosely bound $^3_\Sigma$H structure and the high-energy continuum of the Λnp system is small, resulting in relatively narrow widths of these states. Another crucial aspect of the (meta)stability of Σ^0–^{2}H states is their isospin content, which differs from the dominant T=0 component in the Λ–^{2}H system.

The pole trajectories, however, depend strongly on the chosen *YN* interaction. Among the tested models, the NLO19 interaction with the largest regulator cutoff, λ=700 MeV, is closest to generate Feshbach resonance below Σ^0–^{2}H threshold, whereas the LO model with the smallest cutoff, λ=550 MeV, requires the most substantial modification. This trend, corroborated by cross-section calculations, indicates that the NLO19 λ=700 MeV model is the most favorable for revealing the resonance, while the LO λ=550 MeV model is the least favorable. Despite the differences in trajectories, the real part of the resonance energy for the physical case (γ=1) consistently lies in the vicinity of the Σ^+nn threshold. However, interpreting the resonance solely from its energy position is misleading since the complex energy plane is structured by multiple thresholds and intricate multi-sheet topology. A more transparent picture emerges from analyzing the pole trajectories in the complex momentum plane, as illustrated in Fig. 2. Here, the pole trajectories are traced in the relative Σ^0–^{2}H momentum plane. The physical region is marked by red lines, with the positive real (imaginary) axis indicating energies above (below) the Σ^0–^{2}H threshold. As γ decreases, the poles recede from the physical region, particularly from the Σ^+nn threshold. Consequently, in the complex energy plane the pole resides on a Riemann sheet not directly connected to the physical Σ^0–^{2}H scattering region. In this situation, the parameter $\Gamma = -2E_i$ cannot be interpreted as a conventional resonance width since for $E_R > 0$ only the near-threshold tail of the resonance has physical impact. Instead, one may introduce an

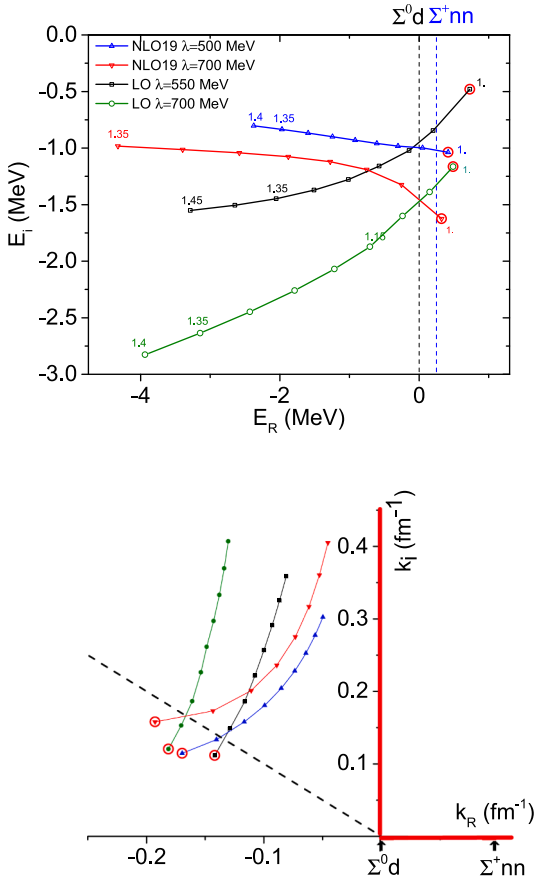

Fig. 2. The ${}^{3}_{\Sigma}$H $J^{\pi}=1/2^{+}$ pole trajectories obtained for different YN interaction models, when varying the strength of ΣN interaction. Trajectories are represented in complex energy (upper panel) and momentum (lower panel) planes, calculated relative to the Σ^0–^{2}H threshold, respectively. The momentum angle $\theta_k = 135$ deg (dashed line) corresponds to $E_R = 0$ in the energy plane.

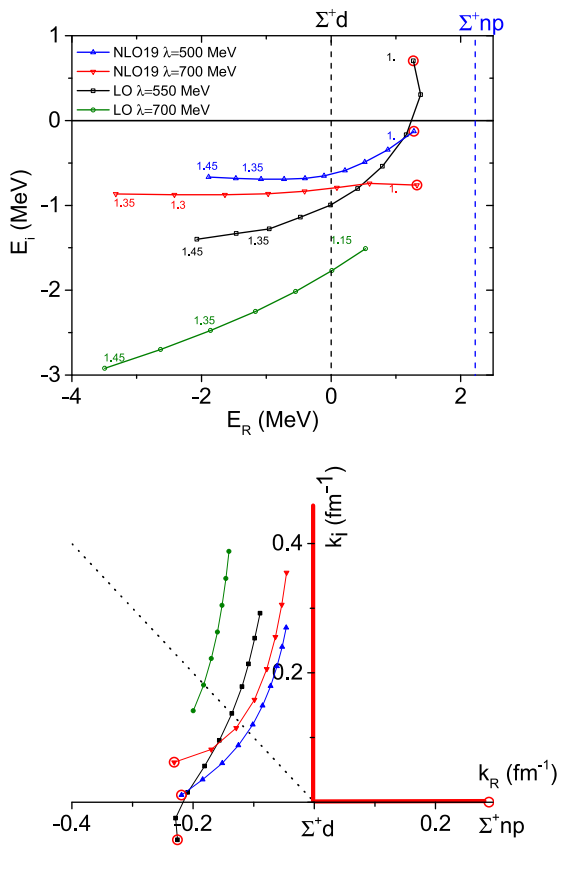

Fig. 3. The ${}^{3}_{\Sigma}$He $J=1/2^{+}$ resonant state trajectories obtained for different YN interaction models, when varying the strength of ΣN interaction. Trajectories represented in energy and momentum, calculated relative to Σ^+–^{2}H threshold, respectively.

effective width $\Gamma_{\rm eff} = 2(E_R^2 + E_i^2)^{1/2}$ where $\Gamma_{\rm eff}/2$ measures the shortest distance in the energy plane from the pole to the physical region, the threshold in this case, in the same way as $\Gamma/2$ does for standard resonances. The influence of such resonant states on observables therefore depends sensitively on the pole position relative to the physical domain, and thus on the delicate interplay between their real and imaginary parts. An example is given in Fig. 1, where the proximity of the resonance to the Σ^0–^{2}H threshold produces a broad peak in the Λ–^{2}H total cross section.

Now, let us explore the potential existence of three-particle Σ-hypernuclear resonance states with charges Z=0 and Z=2. Although these are isospin mirror systems, the substantial difference in the masses of charged Σ baryons results in markedly distinct threshold structures leading to significant differences in the dynamics of resonant states. Again, the NLO19 model with λ=700 MeV requires the smallest scaling to position the centroid of the $J^{\pi} = 1/2^{+}$ state below the Σ emission threshold. For this model, $\gamma \approx 1.11$ generates resonant states centered at the Σ^0–nn and Σ^+–^{2}H thresholds, respectively. From a technical standpoint, tracking the evolution of the Z=2 state which moves below the Σ^+ –^{2} H two-cluster threshold is more straightforward than for the Z=0 state, which traverses the narrow energy gap between the Σ^0 – nn and Σ^- –^{2} H thresholds. Moreover, the ${}^{3}_{\Sigma}$He resonant state holds more experimental relevance as it could be produced in the ^{3}He$(K^-,\pi^-)^{3}_{\Sigma}$He reaction. For the above mentioned reasons the calculation of the Z=0 state was not attempted at this stage. Fig. 3 shows trajectories of this state as the scaling parameter γ varies. Qualitatively, these trajectories resemble those of the previously studied Z=1 case. While the trajectories notably differ for various interaction models the centroids for $\gamma \to 1$ converge to the same region in the complex-energy plane. This region may seem to be located between the Σ^+ – ^{2}H and Σ^+ – np thresholds, but a closer inspection of the trajectories in the complex-momentum plane reveals that the resonances recede from the physical region, especially from the Σ^+–np threshold.

The energies of resonant states for γ=1 are collected in Table 1 both for Z=1 and Z=2 systems. In most cases $E_R > 0$ which is reflected by the complex-momentum angle θ_k having values from 135 to 195 degrees. It is to be stressed that a small value of Γ does not indicate better experimental observability of the state, as $\Gamma_{\rm eff}/2$ has an appreciable value. This feature, characteristic of multithreshold resonances [59], arises because the poles lie on the unphysical Riemann sheets not adjacent to the physical scattering region. In some cases, such as for the LO $\lambda = 550$ MeV YN interaction, crossing the negative real momentum axis even yields a negative value of Γ.

Conversely, the widths of the obtained states exhibit significant dependence on the chosen YN model, reflecting the very distinct ΣN–ΛN coupling strengths in these models. Notably, the $\Sigma^- p \leftrightarrows \Lambda N$ low-energy cross-sections predicted by the Jülich models [38] conform to the upper bound of the experimental dataset by Engelmann et al. [60], while the previous generation YN interaction models based on one-boson exchange theory [61,62] had the tendency to align with the central values. Ultimately, if nature favors weaker ΣN–ΛN coupling, the ${}^{3}_{\Sigma}$H resonance might be more stable and have more pronounced influence on observables, in particular when they are related to Σ^0–^{2}H production. It is worth noting that the recent analysis of measured femtoscopic correlation functions [63] favors the NLO19 models with the largest

Table 1
Positions of $J^\pi=1/2^+$ Σ-hypernuclear resonant states for total charge Z = 1 and Z = 2 systems relative to the $\Sigma^0-{}^2$H and $\Sigma^+-{}^2$H thresholds, respectively.

	Z = 1 ($\Sigma^0-{}^2$H)				Z = 2 ($\Sigma^+-{}^2$H)			
Model	E_R (MeV)	Γ (MeV)	$\Gamma_{\rm eff}$ (MeV)	θ_k (deg)	E_R (MeV)	Γ (MeV)	$\Gamma_{\rm eff}$ (MeV)	θ_k (deg)
LO550	0.73	0.96	1.70	163	1.27	−1.40	2.90	194
LO700	0.49	2.34	2.54	146	1.74	1.08	3.64	171
NLO450(2013)	−0.02	5.04	5.04	135	1.31	3.66	4.50	153
NLO700(2013)	0.49	3.74	3.87	142	1.53	1.86	3.58	164
NLO500(2019)	0.42	2.08	2.24	146	1.31	0.14	2.62	178
NLO700(2019)	0.34	3.26	3.33	141	1.30	1.50	3.00	165

Table 2
Positions and widths of ${}^4_\Sigma$H and ${}^4_\Sigma$He Feshbach resonant states relative to the $\Sigma^0-{}^3$H and $\Sigma^+-{}^3$H thresholds, respectively. In addition to the energy positions we provide (in %) the estimated particle content of these states. In the last row, known experimental values for the ${}^4_\Sigma$He state are provided.

	${}^4_\Sigma$H			${}^4_\Sigma$He		
Model	E_R (MeV)	Γ (MeV)	P($\Lambda,\Sigma^0,\Sigma^+,\Sigma^-$)	E_R (MeV)	Γ (MeV)	P($\Lambda,\Sigma^0,\Sigma^+,\Sigma^-$)
LO550	−1.60	6.49	1,52,4,43	−2.63	6.18	2,23,74,1
LO700	−2.28	8.26	5,54,4,38	−4.36	7.88	6,23,70,1
NLO450(2013)	−2.97	13.0	23,29,4,45	−3.67	11.6	11,26,61,2
NLO700(2013)	−2.71	9.02	2,47,1,50	−4.19	9.00	2,26,72,0.3
NLO500(2019)	−1.26	6.32	5,46,2,46	−2.38	8.15	5,24,71,0.3
NLO700(2019)	−2.80	8.42	1,50,1,48	−4.27	7.59	1,25,74,0.1
Exp.				$-4.4\pm1.0\pm0.3$	7 ± 2 [22]	
				-2.8 ± 0.7	12.0 ± 1.2 [21]	

cutoffs which in our study provide the most pronounced resonant states.

Resonance wave functions are divergent; however, after the complex scaling transformation they become exponentially decaying. CSM thus provides a wave function normalization procedure, employing biconjugate orthonormalization, and a framework to estimate the averages of physical quantities. These averages represent properties of the internal part of the resonance wave function and are to a large extent independent of the CSM parameter(s). In this manner we were able to study properties of the resonance states situated in the vicinity of the Σ production threshold. The observed Z = 1 and Z = 2 resonances are dominated by the ΣNN components with only marginal admixture of ΛNN particle channels, contributing $\sim 1\,\%$ to the total weight. The Z = 2 resonances are purely isospin T = 1 systems, the admixture of T = 2 ΣNN component represent less than 1 % of its total weight. Its particle content is dominated by the Σ^+np channel that contributes $70-90\,\%$ depending on the YN model.

The structure of Z = 1 resonances is more complex – its Λnp component is almost pure T = 1 state which contributes, depending on the model, $92-99\,\%$ to this particle channel. This feature provides stability of these states against decaying into the $\Lambda-{}^2$H channel and making the three-body decay into $\Lambda+n+p$ dominant. The T = 1 component of ΣNN is the dominant one with $\approx 42-70\,\%$ of the total wave function weight. It is supplemented by the T = 0 ΣNN component at $\approx 20-36\,\%$ level. Particle content of the Z = 1 resonances is split between Σ^+nn and Σ^0np channels with Σ^-pp channel accounting for only $\approx 10\,\%$ of the weight; the contribution of the Λnp channel is marginal.

Additionally, we explored the existence of Σ-resonant states with angular momenta $J\neq1/2^+$, as well as Z = -1 and Z = 3 three-particle systems. However, we did not find any indication of narrow resonant states.

3.2. $A = 4$ hypernuclear resonances

In [16,21,22], a narrow Feshbach resonant state in the ${}^4_\Sigma$He system has been identified few MeV below the $\Sigma^+-{}^3$H threshold. In Table 2, we present results of our calculations for A = 4 ${}^4_\Sigma$H and ${}^4_\Sigma$He states. All considered YN interaction models predict existence of narrow $J^\pi=0^+$ Feshbach resonance states in both systems. We also verified that NNN forces mainly shift the threshold energies due to the modified trinucleon binding energies, but have only a minor impact (within 2 %) on the relative positions of the hypernuclear states. This effect, observed in [43,44] for Λ hypernuclei, is attributed to the weak binding of hypernuclei and, consequently, peripheral distribution of the hyperons.

Regarding the structure of these states, the ${}^4_\Sigma$He resonance state is predominantly composed of the Σ^+nnp particle channel, which constitutes approximately $70-74\,\%$ of the wave function. This is supplemented by $\approx 22-26\,\%$ Σ^0npp admixture. In contrast, the ${}^4_\Sigma$H state is distributed almost equally over the Σ^0nnp and Σ^-npp components. The isospin mirror symmetry is not perfectly preserved in these systems, as anticipated by the significant mass differences of Σ hyperons, which exceeds their binding energy in the trinucleon. It is energetically costly to produce a heavy Σ^- baryon, hence the weight of the Σ^-npp component is reduced by half in ${}^4_\Sigma$H compared to its isospin mirror state Σ^+nnp in ${}^4_\Sigma$He.

Calculated locations and widths of these states are strongly YN interaction model dependent. This sensitivity highlights the potential of these systems to deepen our understanding of YN interactions. Importantly, the positions and widths are not directly correlated: the state's position is primarily governed by the ΣN interaction, while the width reflects the strength of $\Lambda N-\Sigma N$ coupling. Unfortunately, large uncertainties in the available experimental data hinder a definitive assessment of the reliability of current YN interaction models. Notably, all models predict the ${}^4_\Sigma$He state within the experimental error bars. A significant discrepancy remains, though, in its measured width [21,22]. Our calculations agree better with a more recent value reported in [22].

In contrast, no resonant states have been identified with $J^\pi\neq0^+$. We have also found no signs of narrow resonance states in Z = 0 and Z = 3 systems, specifically in Σ^0nnn and Σ^0ppp. The absence of these states can be attributed to two obvious reasons: first, the three-neutron (three-proton) system is repulsive due to Pauli blocking; second, the isospin T = 3/2 YN interaction is less attractive than in the T = 1/2 channel.

4. Conclusions

For the first time, rigorous 3- and 4-body calculations have been performed to explore the possible existence of resonant states in A=3, 4 strangeness S = -1 hypernuclear systems, using realistic state-of-the-art NN, NNN and YN interactions derived from χEFT. The coupled-channel nature of YN interactions, as well as the baryon mass differences were fully considered.

We have predicted the existence of $J^\pi = 1/2^+$ Feshbach resonant states in Σnp, Σnn and Σpp systems above the $\Sigma^0 - {}^2$H threshold. We verified that details of the NN interaction models, strongly constrained by NN data, have only a marginal impact on the positions and properties of these resonant states. However, these states exhibit a considerable sensitivity to the YN interaction model. Despite the complex structure of these states, situated above the Σ-hyperon production threshold, they have a significant impact on physical observables. This supports their unambiguous identification in forthcoming experiments.

Despite the considerable uncertainties in the YN interaction models, all models agree on the existence of $J^\pi = 0^+$ Feshbach resonant states in ${}^4_\Sigma$H and ${}^4_\Sigma$He. The strong sensitivity of the identified resonant states to the details of YN interaction, particularly to the less constrained strength of the $\Sigma N - \Lambda N$ coupling, can be exploited to refine our understanding of these interactions.

Finally, we have found no evidence of A = 3 resonant states in Z = −1 and Z = 3 systems, nor in A = 4 systems besides the aforementioned ${}^4_\Sigma$He and ${}^4_\Sigma$H $J^\pi = 0^+$ states. Our results align with Harada's earlier calculations [64], which, using the folding approximation, identified narrow ${}^4_\Sigma$H and ${}^4_\Sigma$He states below the Σ production threshold. On the other hand, Harada also suggested the existence of quasibound ΣNN states, conflicting with our calculations that place these states above the Σ production threshold. Our conclusion however is in agreement with other studies considering full 3-body dynamics but relying on isospin approximation [19,65].

Data availability

Data will be made available on request.

Declaration of competing interest

The authors declare that they have no known competing financial interests or personal relationships that could have appeared to influence the work reported in this paper.

Ackowledgment

We are grateful to J. Haidenbauer and A. Nogga for providing the YN potentials and helping us with their implementation. We were granted access to the HPC resources of TGCC/IDRIS under the allocation 2023-AD010506006R2 made by GENCI (Grand Equipement National de Calcul Intensif). This work was supported by French IN2P3 for a theory project "PUMA", the Research Council of Lithuania (LMTLT) under Contract No. S-MIP-25-15, and by the Czech Science Foundation GAČR Grants No. 25-15746O (M.S.) and 25-18335S (D.G.).

References

[1] A. Gal, E.V. Hungerford, D.J. Millener, Rev. Mod. Phys. 88 (2016) 035004.
[2] M.A. Lisa, S. Pratt, R. Soltz, U. Wiedemann, Annu. Rev. Nucl. Part. Sci. 55 (2005) 357.
[3] L. Tolos, L. Fabbietti, Prog. Part. Nucl. Phys. 112 (2020) 103770.
[4] T.R. Saito, et al., Nature Rev. Phys. 3 (2021) 803.
[5] C. Rappold, et al., Phys. Rev. C 88 (2013) 041001.
[6] J. Adam, et al., Nat. Phys. 16 (2020) 409.
[7] M. Abdallah, et al., Phys. Rev. Lett. 128 (2022) 202301.
[8] S. Acharya, et al., Phys. Rev. Lett. 131 (2023) 102302.
[9] J. Dabrowski, Phys. Rev. C 8 (1973) 835.
[10] I. Afnan, B.F. Gibson, Phys. Rev. C 40 (1989).
[11] J. Haidenbauer, U.-G. Meißner, A. Nogga, Few Body Syst. 62 (2021) 105.
[12] B.F. Gibson, D.R. Lehman, Phys. Rev. C, 23, 404, 1981. American Physical Society.
[13] A. Nogga, H. Kamada, W. Glöckle, Phys. Rev. C, 88, 172501, American Physical Society, 2002.
[14] D. Gazda, A. Gal, Phys. Rev. Lett. 116 (2016) 122501.
[15] H. Le, J. Haidenbauer, U.-G.M. ner, A. Nogga, Phys. Rev. C 107 (2023) 024002.
[16] R. Hayano, T. Ishikawa, M. Iwasaki, H. Outa, E. Takada, H. Tamura, A. Sakaguchi, M. Aoki, T. Yamazaki, Phys. Lett. B 231 (1989) 355.
[17] T. Harada, S. Shinmura, Y. Akaishi, H. Tanaka, Nucl. Phys. A 507 (1990) 715.
[18] B.F. Gibson, I. Afnan, Nucl. Phys. A 547 (1992) 191.
[19] B.F. Gibson, I.R. Afnan, EPJ Web Conf. 271 (2022) 02004.
[20] B. Pandey, rm et al., Phys. Rev. C 105 (2022) 51001.
[21] H. Outa, T. Yamazaki, M. Iwasaki, R.S. Hayano, Prog. Theor. Phys. Suppl. 117 (1994) 177.
[22] T. Nagae, et al., Phys. Rev. Lett. 80 (1998) 1605.
[23] ALICE-collaboration, Reports ALICE-PUBLIC-2020-005, LHCC-G-179, 2020.
[24] M. Fujita, et al., Technical Report, J-PARC, unpublished.
[25] T. Yamaga, et al., Phys. Rev. C 102 (2020) 044002.
[26] S. Merkuriev, Ann. Phys. 130 (1980) 395.
[27] E. Alt, P. Grassberger, W. Sandhas, Nucl. Phys. B 2 (1967) 167.
[28] O.A. Yakubovsky, Sov. J. Nucl. Phys. 5 (1967) 937.
[29] A. Deltuva, A.C. Fonseca, P.U. Sauer, Phys. Lett. B 660 (2008) 471.
[30] A. Deltuva, Phys. Rev. C 88 (2013) 11601.
[31] A. Deltuva, D. Jurčiukonis, Phys. Lett. B 840 (2023) 137867.
[32] R. Lazauskas, Hdr thesis, U. Strasbourg, 2019.
[33] A. Deltuva, Phys. Rev. C 97 (2018) 034001.
[34] A. Deltuva, Europhys. Lett. 95 (2011) 43002.
[35] R. Lazauskas, Few Body Syst., 64, 2023.
[36] H. Polinder, J. Haidenbauer, U.-G. Meissner, Nucl. Phys. A 779 (2006) 244.
[37] J. Haidenbauer, S. Petschauer, N. Kaiser, U.G. Meissner, A. Nogga, W. Weise, Nucl. Phys. A 915 (2013) 24.
[38] J. Haidenbauer, U.G. Meißner, A. Nogga, Eur. Phys. J. A 56 (2020) 91.
[39] D.R. Entem, R. Machleidt, Phys. Rev. C 68 (2003) 041001.
[40] R.B. Wiringa, V.G.J. Stoks, R. Schiavilla, Phys. Rev. C 51 (1995) 38.
[41] R. Machleidt, Phys. Rev. C 63 (2001) 024001.
[42] P. Reinert, H. Krebs, E. Epelbaum, Eur. Phys. J. A 54 (2018) 86.
[43] A. Nogga, H. Kamada, W. Glöckle, Phys. Rev. Lett. 88 (2002) 172501.
[44] D. Gazda, T.Y. Htun, C. Forssén, Phys. Rev. C 106 (2022) 054001.
[45] H. Le, J. Haidenbauer, U.-G.M. ner, A. Nogga, Eur. Phys. J. A 60 (2024) 3.
[46] L. Marcucci, A. Kievsky, S. Rosati, R. Schiavilla, M. Viviani, Phys. Rev. Lett. 121 (2018) 049901.
[47] V. Belyaev, S. Rakityansky, W. Sandhas, Nucl. Phys. A 803 (2008) 210.
[48] E. Hiyama, S. Ohnishi, B. Gibson, T.A. Rijken, Phys. Rev. C 89 (2014) 061302.
[49] A. Gal, H. Garcilazo, Phys. Lett. B 736 (2014) 93.
[50] I.R. Afnan, B.F. Gibson, Phys. Rev. C 92 (2015) 054608.
[51] M. Schäfer, B. Bazak, N. Barnea, J. Mareš, Phys. Lett. B 808 (2020) 135614.
[52] P. Naidon, S. Endo, Rept. Prog. Phys. 80 (2017) 056001.
[53] A. Deltuva, Phys. Rev. C 102 (2020) 034003.
[54] A. Hemmdan, W. Glöckle, H. Kamada, Phys. Rev. C 66 (2002) 054001.
[55] R. Lazauskas, J. Carbonell, Phys. Rev. C 71 (2005) 044004.
[56] R. Lazauskas, J. Carbonell, Phys. Rev. C 72 (2005) 034003.
[57] T. Kraemer, Nature 440 (2006) 315.
[58] J. Stecher, J.P. D'incao, C.H. Greene, Nat. Phys. 5 (2009) 417.
[59] A. Badalyan, L. Kok, M. Polikarpov, Y.A. Simonov, Phys. Rep. 82 (1982) 31.
[60] R. Engelmann, H. Filthuth, V. Hepp, E. Kluge, Phys. Lett. 21 (1966) 587.
[61] T.A. Rijken, V. Stoks, Y. Yamamoto, Phys. Rev. C 59 (1999) 21.
[62] J. Haidenbauer, U.-G. Meißner, Phys. Rev. C 72 (2005) 044005.
[63] S. Acharya, et al., Phys. Lett. B 833 (2022) 137272.
[64] T. Harada, Nucl. Phys. A 672 (2000) 181.
[65] H. Garcilazo, A. Valcarce, Symmetry 14 (2022) 2381.